ELSEVIER

International Journal of Solids and Structures 41 (2004) 3031–3051

INTERNATIONAL JOURNAL OF SOLIDS and STRUCTURES

www.elsevier.com/locate/ijsolstr

Natural frequencies of heated annular and circular plates

Haider N. Arafat, Ali H. Nayfeh*, Waleed Faris

Department of Engineering Science and Mechanics, MC 0219, Virginia Polytechnic Institute and State University, Blacksburg, VA 24061, USA

Received 16 July 2003; received in revised form 8 December 2003

Available online 29 January 2004

Abstract

The behavior of annular plates with clamped–clamped immovable boundary conditions subjected to axisymmetric in-plane thermal loads is considered. The plate is modeled using a linear form of the von Kármán plate theory and the radial temperature distribution is determined from the steady-state heat conduction equation. A numerical shooting method is used to calculate the mode shapes and natural frequencies and the influence of key thermal and geometric parameters on the free vibrations and buckling of the annulus is investigated. Further, an approximate closed-form expression for the natural frequencies is introduced and its validity is explored by comparing its results with those obtained numerically. As a special case, the behavior of clamped thermally loaded circular plates is also investigated.
© 2004 Elsevier Ltd. All rights reserved.

Keywords: Annular plates; Thermal load; Vibrations; Buckling; Natural frequencies

1. Introduction

Plates are key components in many structural and machinery applications. Some examples include turbines, tanks, automotive braking systems, and, more recently, microelectromechanical system (MEMS) devices, such as sensors and micropumps. In many of these applications, the plates are subjected to thermal loads, which may cause buckling and/or induce unexpected dynamic responses. In fact, as early as the 1920s, von Freudenreich (1925) experimentally investigated vibrations in steam turbine disks and matched his results with the theory presented by Stodola (1924). As indicated in the review by Thornton (1993), the thermal buckling of plates and shells has been the subject of much research in the past 50 some years. However, the analysis of the dynamic responses of annular plates subjected to thermal loads has received little attention.

In a series of papers, Mote (1965, 1966, 1967) investigated the influence of inducing thermal membrane stresses in circular saws in an effort to increase their natural frequencies and hence, improve their stability. Fedorov (1976) examined the linear thermostability problem of elastically clamped variable-stiffness

* Corresponding author. Tel.: +1-540-231-5453; fax: +1-540-231-2290.
E-mail address: anayfeh@vt.edu (A.H. Nayfeh).

0020-7683/$ - see front matter © 2004 Elsevier Ltd. All rights reserved.
doi:10.1016/j.ijsolstr.2003.12.028

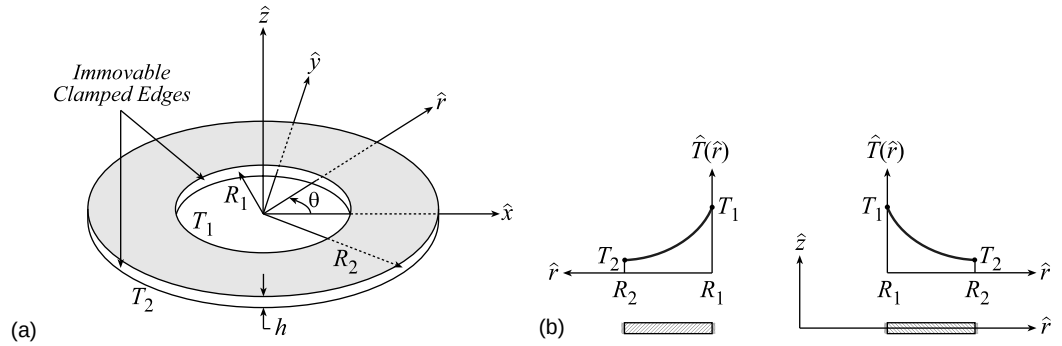

Fig. 1. A schematic of (a) an annular plate and (b) a cross-sectional view illustrating a typical steady-state axisymmetric temperature distribution.

annular plates under axisymmetric radial nonuniform thermal loads. He found that, in certain cases, variations of the Young modulus and the Poisson ratio with temperature cannot be neglected. Irie and Yamada (1978) investigated the linear free vibrations of elastically supported circular and annular plates, with one edge exposed to an axisymmetric sinusoidal heat flux and the other edge thermally insulated. More recently, the nonlinear free vibrations of isotropic and axisymmetric orthotropic annular plates carrying concentric rigid masses and subject to thermal loads were investigated by Li et al. (2002). They modeled the plates using the von Kármán equations and assumed the nonlinear responses to be harmonic. They then applied the Kantorovich averaging method and examined the nonlinear natural frequencies and thermal buckling loads for hinged and clamped immovable boundary conditions. In all of the aforementioned works, the temperature distribution was found to be a significant parameter affecting the free response.

In this work, the free vibrations and buckling of annular plates with clamped–clamped immovable boundary conditions subjected to axisymmetric in-plane thermal loads are analyzed (see Fig. 1). A linearized version of the von Kármán plate theory is used to model the behavior of the annular plates and explore the influence of several thermal and geometric parameters on the system response. The natural frequencies and mode shapes are calculated numerically by a shooting method. In addition, the method of strained parameters is applied to determine an approximate closed-form expression for the natural frequencies. The free vibrations and buckling of thermally loaded circular plates are also investigated as a special case.

2. Problem formulation

The linear undamped free vibrations of an annular plate under an axisymmetric thermal load are governed by

$$D\hat{\nabla}^4\hat{w}+\rho h\frac{\partial^2\hat{w}}{\partial\hat{t}^2}=\frac{\partial^2\hat{w}}{\partial\hat{r}^2}\left(\frac{1}{\hat{r}}\frac{\partial\widehat{F}}{\partial\hat{r}}+\frac{1}{\hat{r}^2}\frac{\partial^2\widehat{F}}{\partial\theta^2}\right)+\frac{\partial^2\widehat{F}}{\partial\hat{r}^2}\left(\frac{1}{\hat{r}}\frac{\partial\hat{w}}{\partial\hat{r}}+\frac{1}{\hat{r}^2}\frac{\partial^2\hat{w}}{\partial\theta^2}\right)-2\left(\frac{1}{\hat{r}}\frac{\partial^2\widehat{F}}{\partial\hat{r}\partial\theta}-\frac{1}{\hat{r}^2}\frac{\partial\widehat{F}}{\partial\theta}\right)\left(\frac{1}{\hat{r}}\frac{\partial^2\hat{w}}{\partial\hat{r}\partial\theta}-\frac{1}{\hat{r}^2}\frac{\partial\hat{w}}{\partial\theta}\right)-\frac{1}{(1-\nu)}\hat{\nabla}^2\widehat{M}_T, \tag{1}$$

$$k\hat{\nabla}^2\widehat{T}+\widehat{Q}=\rho c_p\frac{\partial\widehat{T}}{\partial\hat{t}}+\frac{E\alpha T_0}{1-2\nu}\frac{\partial e}{\partial\hat{t}}, \tag{2}$$

where

$$\widehat{M}_T = E\alpha \int_{-\frac{h}{2}}^{\frac{h}{2}} \left[\widehat{T}(\hat{r},\hat{t}) - T_0\right]\hat{z}\,\mathrm{d}\hat{z} = 0 \tag{3}$$

and the biharmonic operator is given by

$$\hat{\nabla}^4 = \hat{\nabla}^2\hat{\nabla}^2 = \left(\frac{\partial^2}{\partial\hat{r}^2} + \frac{1}{\hat{r}}\frac{\partial}{\partial\hat{r}} + \frac{1}{\hat{r}^2}\frac{\partial^2}{\partial\theta^2}\right)\left(\frac{\partial^2}{\partial\hat{r}^2} + \frac{1}{\hat{r}}\frac{\partial}{\partial\hat{r}} + \frac{1}{\hat{r}^2}\frac{\partial^2}{\partial\theta^2}\right). \tag{4}$$

Here, $\hat{r}$ and θ are polar coordinates; $\hat{t}$ is time; $\hat{w}$ is the plate transverse displacement; $\widehat{F}$ is the stress function; $\widehat{T}$ is the axisymmetric temperature distribution; T_0 is the initial stress-free temperature; ρ is the material density; h is the plate thickness; e is the dilatational strain due to the thermal effect; c_p is the heat capacity coefficient at constant pressure; α is the coefficient of thermal expansion; k is the thermal conductivity; E is the modulus of elasticity; v is Poisson's ratio; and $D = \frac{Eh^3}{12(1-v^2)}$ is the bending rigidity. In this paper, we consider the case in which the heat flux $\widehat{Q} = 0$.

Newman and Forray (1962) used von Kármán's plate theory to formulate the problem of nonlinear axisymmetric static deflections of circular plates under thermal and mechanical loads. Using a finite-difference scheme, they then investigated the case of a simply-supported immovable plate. For the linear compatibility relation, we follow the approach of Newman and Forray (1962) and note that

$$\epsilon_r = \frac{1}{Eh}\left(\widehat{N}_r - v\widehat{N}_\theta\right) + \alpha(\widehat{T} - T_0), \tag{5}$$

$$\epsilon_\theta = \frac{1}{Eh}\left(\widehat{N}_\theta - v\widehat{N}_r\right) + \alpha(\widehat{T} - T_0), \tag{6}$$

$$\widehat{N}_r = \frac{1}{\hat{r}}\frac{\partial\widehat{F}}{\partial\hat{r}} + \frac{1}{\hat{r}^2}\frac{\partial^2\widehat{F}}{\partial\theta^2} \quad \text{and} \quad \widehat{N}_\theta = \frac{\partial^2\widehat{F}}{\partial\hat{r}^2}, \tag{7}$$

$$\epsilon_r = \frac{\partial\hat{u}}{\partial\hat{r}} \quad \text{and} \quad \epsilon_\theta = \frac{\hat{u}}{\hat{r}} + \frac{1}{\hat{r}}\frac{\partial\hat{v}}{\partial\theta}, \tag{8}$$

where $\hat{u}$ and $\hat{v}$ are the radial and hoop displacements, respectively. Because the temperature distribution considered here is axisymmetric, the stress function and in-plane displacements are also assumed to be so; that is, $\frac{\partial}{\partial\theta}(\widehat{F},\hat{u},\hat{v}) = (0,0,0)$. Therefore, it follows from Eqs. (5)–(8) that

$$\frac{\partial\hat{u}}{\partial\hat{r}} = \frac{1}{Eh}\left(\frac{1}{\hat{r}}\frac{\partial\widehat{F}}{\partial\hat{r}} - v\frac{\partial^2\widehat{F}}{\partial\hat{r}^2}\right) + \alpha(\widehat{T} - T_0), \tag{9}$$

$$\frac{\hat{u}}{\hat{r}} = \frac{1}{Eh}\left(\frac{\partial^2\widehat{F}}{\partial\hat{r}^2} - \frac{v}{\hat{r}}\frac{\partial\widehat{F}}{\partial\hat{r}}\right) + \alpha(\widehat{T} - T_0). \tag{10}$$

Then, after eliminating $\hat{u}$ from Eqs. (9) and (10), we obtain the compatibility equation

$$\hat{r}\frac{\partial^3\widehat{F}}{\partial\hat{r}^3} + \frac{\partial^2\widehat{F}}{\partial\hat{r}^2} - \frac{1}{\hat{r}}\frac{\partial\widehat{F}}{\partial\hat{r}} = -Eh\alpha\hat{r}\frac{\partial\widehat{T}}{\partial\hat{r}}. \tag{11}$$

Moreover, because of the axisymmetry of $\widehat{F}$ and after using Eq. (3), we reduce Eq. (1) to the following form:

$$D\hat{\nabla}^4\hat{w} + \rho h\frac{\partial^2\hat{w}}{\partial\hat{t}^2} = \frac{\partial^2\widehat{F}}{\partial\hat{r}^2}\left(\frac{1}{\hat{r}}\frac{\partial\hat{w}}{\partial\hat{r}} + \frac{1}{\hat{r}^2}\frac{\partial^2\hat{w}}{\partial\theta^2}\right) + \frac{1}{\hat{r}}\frac{\partial^2\hat{w}}{\partial\hat{r}^2}\frac{\partial\widehat{F}}{\partial\hat{r}}. \tag{12}$$

Because from Eq. (11), the stress function $\widehat{F}$ is independent of the displacement $\hat{w}$, Eq. (12) is a linear partial-differential equation with variable coefficients for $\hat{w}$.

The associated boundary conditions for a clamped–clamped annular plate are as follows:

$$\hat{w} = 0 \quad \text{and} \quad \frac{\partial\hat{w}}{\partial\hat{r}} = 0 \quad \text{at } \hat{r} = R_1, R_2, \tag{13}$$

$$\widehat{T} = T_1 \quad \text{at } \hat{r} = R_1, \tag{14}$$

$$\widehat{T} = T_2 \quad \text{at } \hat{r} = R_2, \tag{15}$$

where R_1 and R_2 are the inner and outer radii, respectively, and T_1 and T_2 are constant temperatures. In addition, because both of the inner and outer boundaries are assumed to be immovable, the radial deflection $\hat{u}$ must vanish at $\hat{r} = R_1$ and R_2. Hence, it follows from Eq. (10) that

$$\frac{\partial^2\widehat{F}}{\partial\hat{r}^2} - \frac{v}{\hat{r}}\frac{\partial\widehat{F}}{\partial\hat{r}} + Eh\alpha(\widehat{T} - T_0) = 0 \quad \text{at } \hat{r} = R_1, R_2. \tag{16}$$

3. Solution procedure

The terms on the right-hand side of Eq. (2) represent, respectively, the diffusion of heat and thermoelastic coupling (Hetnarski, 1987). As discussed by Boley and Weiner (1960), the thermoelastic coupling term is typically relevant to problems where the response is affected by heat dissipation through the body. In this case, the heat dissipation occurs at a much slower rate compared to the vibrations of the plate, and hence the effects of these terms may be neglected and Eq. (2) reduces to

$$\hat{\nabla}^2\widehat{T} = 0. \tag{17}$$

The solution of Eqs. (14), (15), and (17) yields the following temperature distribution:

$$\widehat{T}(\hat{r}) = \frac{1}{(\ln R_2 - \ln R_1)}\Big[(T_1\ln R_2 - T_2\ln R_1) - (T_1 - T_2)\ln\hat{r}\Big]. \tag{18}$$

Next, we substitute Eq. (18) into Eq. (11) and obtain the equation governing the stress function $\widehat{F}$ as

$$\hat{r}\frac{\partial^3\widehat{F}}{\partial\hat{r}^3} + \frac{\partial^2\widehat{F}}{\partial\hat{r}^2} - \frac{1}{\hat{r}}\frac{\partial\widehat{F}}{\partial\hat{r}} = Eh\alpha\Lambda, \tag{19}$$

where

$$\Lambda = \frac{T_2 - T_1}{\ln R_1 - \ln R_2}. \tag{20}$$

The solution of Eqs. (16) and (19) is

$$\widehat{F}(\hat{r}) = \widehat{C}_1\hat{r}^2 + \widehat{C}_2\ln\hat{r} + \widehat{C}_3 + \frac{1}{4}Eh\alpha\Lambda\hat{r}^2(\ln\hat{r} - 1), \tag{21}$$

where $\widehat{C}_3$ is arbitrary and

$$\widehat{C}_1 = \frac{Eh\alpha}{8(1-\nu)}\left\{\frac{4R_2^2(T_2-T_0)}{R_1^2-R_2^2} - \frac{4R_1^2(T_1-T_0)}{R_1^2-R_2^2} + \frac{\Lambda R_2^2[1+\nu+2(1-\nu)\ln R_2]}{R_1^2-R_2^2} - \frac{\Lambda R_1^2[1+\nu+2(1-\nu)\ln R_1]}{R_1^2-R_2^2}\right\}, \tag{22}$$

$$\widehat{C}_2 = -\frac{1}{2}Eh\alpha\frac{R_1^2R_2^2(T_1-T_2)}{R_1^2-R_2^2}. \tag{23}$$

We then substitute Eq. (21) into Eq. (12) and obtain the following equation governing the free undamped vibrations of an annular plate under an axisymmetric thermal load:

$$D\hat{\nabla}^4\hat{w} + \frac{1}{\hat{r}}\frac{\partial}{\partial\hat{r}}\left[\widehat{L}_1(\hat{r})\frac{\partial\hat{w}}{\partial\hat{r}}\right] + \frac{1}{\hat{r}^2}\widehat{L}_2(\hat{r})\frac{\partial^2\hat{w}}{\partial\theta^2} + \rho h\frac{\partial^2\hat{w}}{\partial\hat{t}^2} = 0, \tag{24}$$

where

$$\widehat{L}_1(\hat{r}) = -2\widehat{C}_1\hat{r} - \frac{\widehat{C}_2}{\hat{r}} - \frac{Eh\alpha\Lambda}{4}\hat{r}(2\ln\hat{r}-1), \tag{25}$$

$$\widehat{L}_2(\hat{r}) = \frac{\mathrm{d}\widehat{L}_1}{\mathrm{d}\hat{r}} = -2\widehat{C}_1 + \frac{\widehat{C}_2}{\hat{r}^2} - \frac{Eh\alpha\Lambda}{4}(2\ln\hat{r}+1) \tag{26}$$

and subject to the boundary conditions in Eq. (13).

4. Nondimensional problem

To better understand the problem at hand and ascertain the critical parameters influencing the response behavior, we introduce the following nondimensional variables and parameters:

$$r = \frac{\hat{r}}{R_2}, \quad t = \frac{1}{R_2^2}\sqrt{\frac{D}{\rho h}}\hat{t}, \quad \Delta T = \frac{\widehat{T}-T_0}{T_2-T_0}, \quad w = \frac{\hat{w}}{h}, \quad \tau = \frac{T_1-T_0}{T_2-T_0}, \quad b = \frac{R_1}{R_2}. \tag{27}$$

Consequently, Eqs. (13) and (24) become

$$\nabla^4 w + p\left\{\frac{1}{r}\frac{\partial}{\partial r}\left[L_1(r)\frac{\partial w}{\partial r}\right] + \frac{1}{r^2}L_2(r)\frac{\partial^2 w}{\partial\theta^2}\right\} + \frac{\partial^2 w}{\partial t^2} = 0, \tag{28}$$

$$w = 0 \quad \text{and} \quad \frac{\partial w}{\partial r} = 0 \quad \text{at } r = b, 1, \tag{29}$$

where ∇^4 is given by Eq. (4) after dropping the hat (^),

$$p = \frac{12(1+\nu)\alpha(T_2-T_0)R_2^2}{h^2} \tag{30}$$

is a measure of the thermal load,

$$L_1(r) = -2C_1 r - \frac{C_2}{r} - \frac{(1-\tau)(1-\nu)}{4\ln b}r(2\ln r - 1), \tag{31}$$

$$L_2(r) = -2C_1 + \frac{C_2}{r^2} - \frac{(1-\tau)(1-\nu)}{4\ln b}(2\ln r + 1) \tag{32}$$

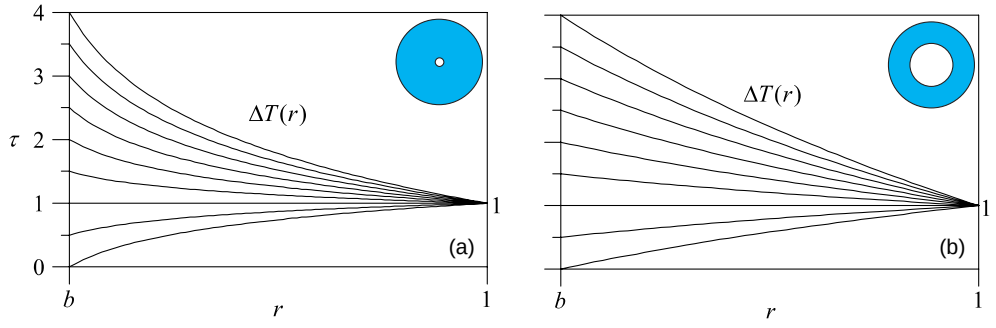

Fig. 2. The nondimensional temperature distribution $\Delta T(r)$ for different values of the temperature ratio τ when (a) $b = 0.1$ and (b) $b = 0.5$.

and

$$C_1 = \frac{\{b^2[(1+\tau) - \nu(1-\tau)] - 2\}}{4(1-b^2)} - \frac{(1+\nu)(1-\tau)}{8\ln b}, \quad C_2 = -\frac{b^2(1-\nu)(1-\tau)}{2(1-b^2)}. \tag{33}$$

From Eqs. (18) and (27), the nondimensional temperature distribution is given by

$$\Delta T(r) = 1 + (\tau - 1)\frac{\ln r}{\ln b} \tag{34}$$

so that $\Delta T(b) = \tau$ and $\Delta T(1) = 1$. In Fig. 2, we show the nondimensional temperature distribution for different absolute temperature ratios τ. We take in part (a) $b = 0.1$ and in part (b) $b = 0.5$. We note that the temperature distribution approaches a linear behavior as the annulus becomes narrower.

5. Eigenvalue problem

Next, we assume a harmonic response of the form

$$w(r,\theta,t) = \sum_{m=1}^{\infty}\sum_{n=-\infty}^{\infty} \phi_{nm}(r)\mathrm{e}^{\mathrm{i}(\omega_{nm}t + n\theta)} \tag{35}$$

and obtain the eigenvalue problem for the nondimensional mode shapes $\phi_{nm}(r)\mathrm{e}^{\mathrm{i}n\theta}$ and corresponding nondimensional natural frequencies ω_{nm} as

$$\tilde{\nabla}^4\phi_{nm} + p\frac{1}{r}\frac{\mathrm{d}}{\mathrm{d}r}\left[L_1(r)\frac{\mathrm{d}\phi_{nm}}{\mathrm{d}r}\right] - \left[p\frac{n^2}{r^2}L_2(r) + \omega_{nm}^2\right]\phi_{nm} = 0, \tag{36}$$

$$\phi_{nm} = 0 \quad \text{and} \quad \frac{\mathrm{d}\phi_{nm}}{\mathrm{d}r} = 0 \quad \text{at } r = b, 1, \tag{37}$$

where

$$\tilde{\nabla}^4 = \left(\frac{\mathrm{d}^2}{\mathrm{d}r^2} + \frac{1}{r}\frac{\mathrm{d}}{\mathrm{d}r} - \frac{n^2}{r^2}\right)\left(\frac{\mathrm{d}^2}{\mathrm{d}r^2} + \frac{1}{r}\frac{\mathrm{d}}{\mathrm{d}r} - \frac{n^2}{r^2}\right). \tag{38}$$

In the notation used here, $n = 0, 1, 2, 3, \ldots$ denotes the number of nodal diameters and $m = 1, 2, 3, \ldots$ denotes the number of nodal circles. Furthermore, the outer boundary is taken as a nodal circle.

In Fig. 3, we present the first few mode shapes of a clamped–clamped annular plate of $b = 0.5$ when $p = 0$. The top three modes ($n = 0$) are axisymmetric, whereas the bottom nine modes ($n \neq 0$) are asym-

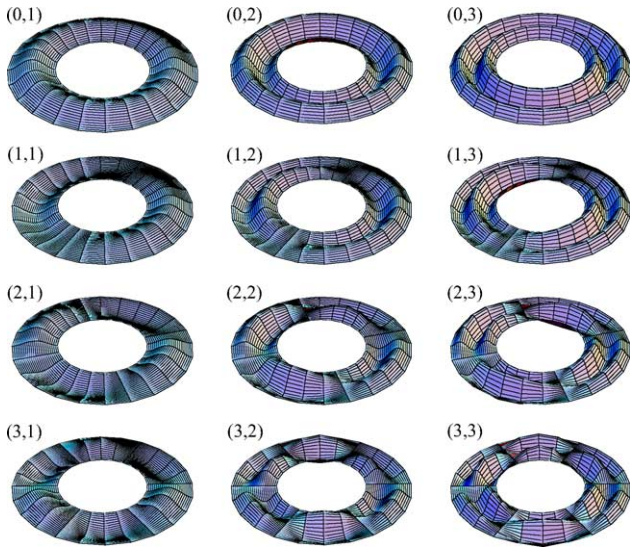

Fig. 3. The first few (n, m) mode shapes of a clamped–clamped annular plate for $b = 0.5$.

metric. When $n \neq 0$, the eigenvalue problem is said to be "degenerate," because two similar mode shapes, which are out of phase by 90° exist for a given natural frequency.

6. Analytical results

Next, we present two cases for which analytical closed-form solutions are available. All of the numerical results we present are for the Poisson ratio $v = 0.3$.

6.1. Case of $\tau = 1$: a zero temperature gradient

When the temperatures at the inner and outer boundaries are equal to each other (i.e., $\tau = 1$), there is no temperature gradient across the annulus, as illustrated in Fig. 2. Setting $\tau = 1$ in Eqs. (31)–(33), we find that $C_2 = 0$, $C_1 = -\frac{1}{2}$, $L_1(r) = r$, and $L_2(r) = 1$. Therefore, Eq. (36) becomes

$$\tilde{\nabla}^4 \phi_{nm} + p\tilde{\nabla}^2 \phi_{nm} - \omega_{nm}^2 \phi_{nm} = 0. \tag{39}$$

The general solution of Eq. (39) can be expressed in terms of Bessel functions as

$$\phi_{nm}(r) = A_1 J_n(\xi_1 r) + A_2 Y_n(\xi_1 r) + A_3 I_n(\xi_2 r) + A_4 K_n(\xi_2 r), \tag{40}$$

where

$$\xi_1 = \sqrt{\frac{1}{2}\left[p + \sqrt{p^2 + 4\omega_{nm}^2}\right]}, \tag{41}$$

$$\xi_2 = \sqrt{\frac{1}{2}\left[-p + \sqrt{p^2 + 4\omega_{nm}^2}\right]}. \tag{42}$$

Substituting Eq. (40) into the boundary conditions, we obtain the following characteristic equation for the natural frequencies:

$$\Delta = \begin{vmatrix} J_n(\xi_1 b) & Y_n(\xi_1 b) & I_n(\xi_2 b) & K_n(\xi_2 b) \\ \xi_1 J_n'(\xi_1 b) & \xi_1 Y_n'(\xi_1 b) & \xi_2 I_n'(\xi_2 b) & \xi_2 K_n'(\xi_2 b) \\ J_n(\xi_1) & Y_n(\xi_1) & I_n(\xi_2) & K_n(\xi_2) \\ \xi_1 J_n'(\xi_1) & \xi_1 Y_n'(\xi_1) & \xi_2 I_n'(\xi_2) & \xi_2 K_n'(\xi_2) \end{vmatrix} = 0, \tag{43}$$

where the prime ($'$) indicates the derivative with respect to the argument $\xi_i r$ for $i = 1, 2$.

In Fig. 4a and b, we present variation of the natural frequencies ω_{nm}, $n = 0, 1, 2, 3$ and $m = 1, 2, 3$, with the thermal load p when $\tau = 1$. The ratio of the inner radius to the outer radius is $b = 0.1$ in Fig. 4a and $b = 0.5$ in Fig. 4b. We note that, for all cases, the natural frequencies monotonously decrease to zero as p increases. The point at which $\omega_{nm} = 0$ corresponds to buckling of the plate in a shape similar to the mode shape $\phi_{nm}(r)e^{in\theta}$.

We can determine the values of p at which buckling occurs by setting $\omega_{nm} = 0$ in Eq. (39) and solving the resulting problem. When $\omega_{nm} = 0$, the general solution of Eq. (39) for $n = 1, 2, 3 \ldots$ is

$$\phi_{nm}(r) = B_1 J_n(\sqrt{p}r) + B_2 Y_n(\sqrt{p}r) + B_3 r^n + \frac{B_4}{r^n} \tag{44}$$

and for $n = 0$ (i.e., axisymmetric modes) is

$$\phi_{0m}(r) = B_1 J_0(\sqrt{p}r) + B_2 Y_0(\sqrt{p}r) + B_3 + B_4 \ln r. \tag{45}$$

Then, substituting Eq. (44) and/or Eq. (45) into the boundary conditions, setting the determinant of the resulting system of algebraic equations equal to zero, and solving for the roots, we obtain the critical buckling loads. The first few buckling loads p_{nm}^* are presented in Table 1 for $b = 0.1$ and 0.5. They are in agreement with the results in Fig. 4a and b.

As the thermal load is increased, modes having the same number of nodal diameters may become involved in internal resonances. For example, we show in Fig. 5 variation of the natural frequencies ω_{01}, ω_{02}, and ω_{03}, corresponding to the first three axisymmetric modes, with p for the cases $b = 0.1$ and 0.5. We find that as p increases, a three-to-one internal resonance $3\omega_{01} \approx \omega_{02}$ may occur at $p \approx 14$ and 42.5, respec-

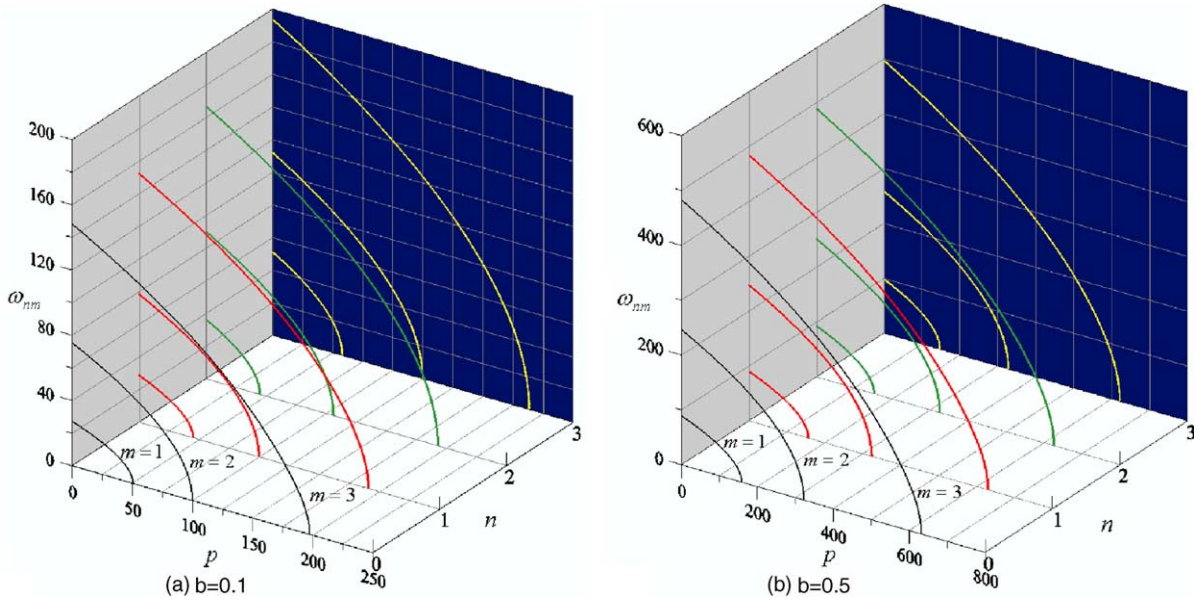

Fig. 4. Variation of the first few natural frequencies ω_{nm} with the thermal load p when $\tau = 1$.

Table 1
Values of the first few critical buckling loads p^*_{nm} of two annular plates for the case $\tau = 1$

n	$b = 0.1$			$b = 0.5$		
	p^*_{n1}	p^*_{n2}	p^*_{n3}	p^*_{n1}	p^*_{n2}	p^*_{n3}
0	50.622	99.986	197.408	158.411	322.918	632.161
1	45.024	99.703	190.769	156.513	323.465	630.243
2	45.089	106.087	192.942	152.140	325.278	625.988
3	58.091	124.762	213.440	148.279	328.809	622.490

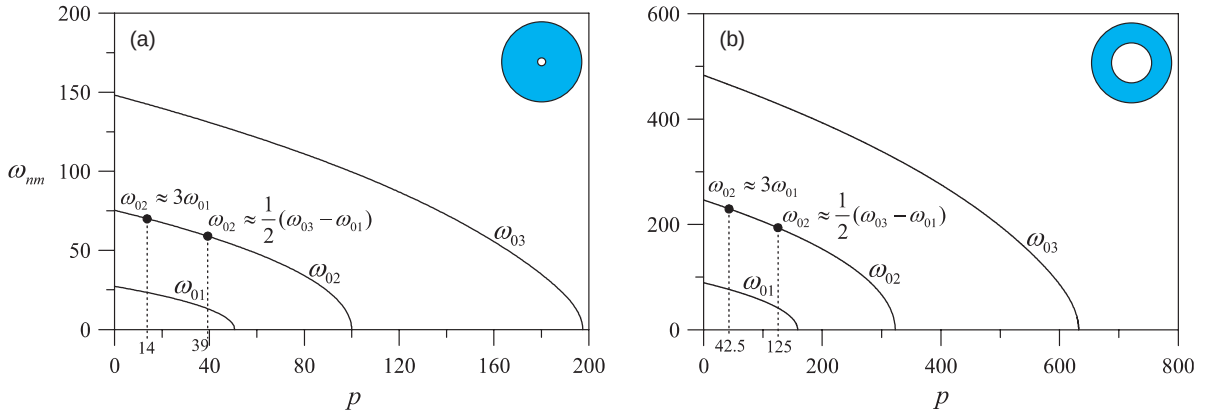

Fig. 5. Variation of the natural frequencies of the first three axisymmetric modes with the thermal load p when $\tau = 1$: (a) $b = 0.1$ and (b) $b = 0.5$.

tively. Furthermore, a combination internal resonance $\frac{1}{2}(\omega_{03} - \omega_{01}) \approx \omega_{02}$ may occur at $p \approx 39$ and 125, respectively.

Similarly, modes having the same number of nodal circles may also become involved in internal resonances as p is increased. Such cases are discussed later.

6.2. Case of $b = 0$: a circular plate

Another case for which closed-form solutions exist is the thermal loading of a circular plate, obtained by setting $b = 0$. Doing so, we again arrive at Eq. (39). This is because it follows from Eq. (18) that in the limit $R_1 \to 0$, the temperature distribution $\widehat{T}(\hat{r}) = T_2$, and hence there is no temperature gradient across the plate. However, for this case, only the boundary conditions at $r = 1$ in Eq. (37) are considered, augmented with the constraint that the deflection must be finite at the origin; that is, $\phi(0) < \infty$. The solution of this problem is given by Eqs. (40)–(42) after setting $A_2 = A_4 = 0$. The characteristic equation governing the natural frequencies is given by

$$\Delta = \begin{vmatrix} J_n(\xi_1) & I_n(\xi_2) \\ \xi_1 J_n'(\xi_1) & \xi_2 I_n'(\xi_2) \end{vmatrix} = 0. \tag{46}$$

In Fig. 6, we show variation of the first few natural frequencies with the thermal load p for a circular plate. Again, we note a monotonic decrease in the ω_{nm} with increasing p. The critical values of p at which buckling occurs can be found by setting $B_2 = B_4 = 0$ in Eq. (44) and/or Eq. (45), satisfying the boundary conditions at $r = 1$, setting the determinant of the resulting system of algebraic equations equal to zero, and

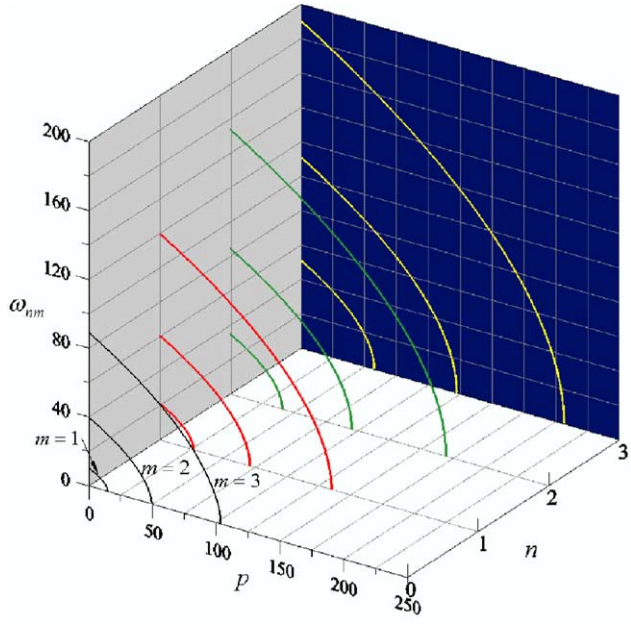

Fig. 6. Variation of the first few natural frequencies ω_{nm} with the thermal load p for the case $b = 0$.

Table 2
Values of the first few critical buckling loads p^*_{nm} of a circular plate (i.e., $b = 0$)

n	p^*_{n1}	p^*_{n2}	p^*_{n3}
0	14.682	49.219	103.499
1	26.375	70.850	135.021
2	40.707	95.278	169.395
3	57.583	122.428	206.570

solving for the roots. The first few buckling loads are presented in Table 2, which are in agreement with the results in Fig. 6.

We note from Table 2 that, for a given number of nodal circles m in the mode shapes, the critical buckling loads significantly vary with the number of nodal diameters n. This is because, for a circular plate at the initial stress-free temperature T_0 (i.e., $p = 0$), the natural frequencies of modes having the same value of m vary considerably with n, as can be seen from Fig. 6. In contrast, in the annular plate, for a given value of b, such critical buckling loads are relatively close to each other, as seen from Table 1. This is because the corresponding natural frequencies at $p = 0$ are also relatively close, as shown in Fig. 4a and b.

With the variation of the thermal load, internal resonances may also be activated in a circular plate. In Fig. 7, we show variation of the natural frequencies of the first three axisymmetric modes. We find that for $p \approx 0.9$, the internal combination resonance $\frac{1}{2}(\omega_{03} - \omega_{01}) \approx \omega_{02}$ may occur. But, we note the absence of the internal resonance $3\omega_{01} \approx \omega_{02}$ in Fig. 7, which was discussed earlier for annular plates, and instead find that $3\omega_{02} \approx \omega_{03}$ for $p \approx 28.5$. In general, these resonances may also be present among other modes having the same value of $n \neq 0$.

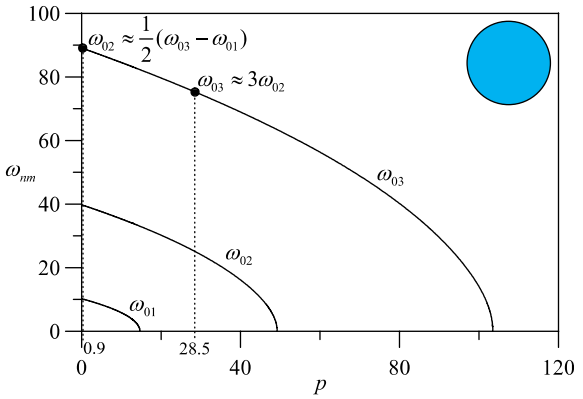

Fig. 7. Variation of the natural frequencies of the first three axisymmetric modes with the thermal load p for the case $b = 0$.

7. General case

Equation (36) is a linear ordinary-differential equation with variable coefficients for the annular plate mode shapes. In general, closed-form solutions of Eq. (36) are not available. Therefore, we use a shooting method to numerically solve the eigenvalue problem. To this end, we form two initial-value problems consisting of Eq. (36) and the boundary conditions at $r = b$ in Eq. (37). We augment the first problem by $\phi''_{nm}(b) = 1$ and $\phi'''_{nm}(b) = 0$ and the second problem by $\phi''_{nm}(b) = 0$ and $\phi'''_{nm}(b) = 1$. Then, for a given value of p, we guess an initial value of ω_{nm}, integrate both problems over $r \in [b, 1]$, and obtain the solutions $\phi^{(1)}_{nm}(r)$ and $\phi^{(2)}_{nm}(r)$. Next, we express the solution of the original eigenvalue problem as a linear combination of both solutions as follows:

$$\phi_{nm}(r) = c_1\phi^{(1)}_{nm}(r) + c_2\phi^{(2)}_{nm}(r), \tag{47}$$

where the c_i are constants. Using Eq. (47) to satisfy the boundary conditions at $r = 1$ in Eq. (37), we arrive at the characteristic equation

$$\phi^{(1)}_{nm}(1)\frac{\mathrm{d}\phi^{(2)}_{nm}(1)}{\mathrm{d}r} - \frac{\mathrm{d}\phi^{(1)}_{nm}(1)}{\mathrm{d}r}\phi^{(2)}_{nm}(1) = 0. \tag{48}$$

Because the initial value of ω_{nm} is simply a guess, this condition is unlikely to be satisfied at first. However, through an iterative procedure, one can converge on the correct value of ω_{nm}. Having done so, we represent the mode shape as

$$\phi_{nm}(r) = c_1\left[\phi^{(1)}_{nm}(r) - \frac{\phi^{(1)}_{nm}(1)}{\phi^{(2)}_{nm}(1)}\phi^{(2)}_{nm}(r)\right], \tag{49}$$

where c_1 is determined so that $\int_b^1 r\phi^2_{nm}(r)\,\mathrm{d}r = 1$. The procedure is then repeated for a different value of p until buckling is reached.

In Fig. 8a and b, we present for $b = 0.1$ and 0.5, respectively, variation of the first few natural frequencies with the thermal load p when $\tau = 2$; that is, the absolute temperature at the inner radius is twice the absolute temperature at the outer radius. The trend in both figures is similar to that in Fig. 4a and b for $\tau = 1$. However, buckling of the plate in this case occurs for smaller values of p. The corresponding buckling loads are presented in Table 3.

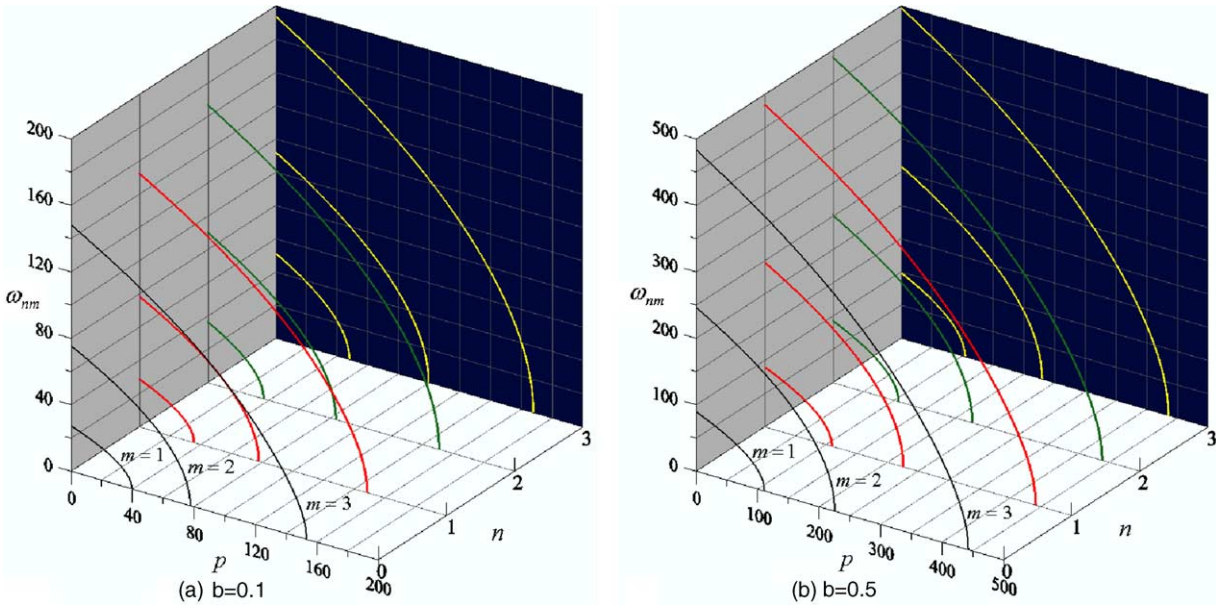

Fig. 8. Variation of the first few natural frequencies ω_{nm} with the thermal load p when $\tau = 2$.

Table 3
Values of the first few critical buckling loads p^*_{nm} of two annular plates for the case $\tau = 2$

n	$b = 0.1$			$b = 0.5$		
	p^*_{n1}	p^*_{n2}	p^*_{n3}	p^*_{n1}	p^*_{n2}	p^*_{n3}
0	39.581	77.624	153.283	110.901	225.423	442.976
1	35.695	77.788	148.515	109.709	225.841	441.552
2	36.594	83.647	150.817	106.995	227.224	438.361
3	48.138	99.612	167.896	104.736	229.905	435.659

In Fig. 9a and b, we present variation of the first few natural frequencies with p when $\tau = 0.5$; that is, the absolute temperature at the inner radius is one-half the absolute temperature at the outer radius. In this case, we find that the critical thermal loads p^*_{nm} at which the plate buckles are greater than those when $\tau = 1$, in contrast to the previous case of $\tau = 2$. These values are presented in Table 4.

8. Approximate closed-form solutions

From the numerical results obtained in Figs. 4, 6, 8, and 9, we note that, for relatively small values of p, the natural frequencies of the higher modes vary almost linearly with p. This point is further illustrated in Fig. 10, where we present variation of the first few natural frequencies ω_{nm} of a circular plate. In part (a), we vary p up to the lowest buckling load $p^*_{01} = 14.682$, and in part (b), we vary p up to 25% of the nmth mode buckling load p^*_{nm}. Following Eq. (40) for the cases of $\tau = 1$ or $b = 0$, we note that in Eq. (39), the term $p\tilde{\nabla}^2\phi_{nm} \propto \xi_i^2\phi_{nm}$ while the term $\tilde{\nabla}^4\phi_{nm} \propto \xi_i^4\phi_{nm}$, where $i = 1, 2$. Defining $\epsilon \equiv \frac{p}{\omega_{nm}}$ in Eqs. (41) and (42), we express the ξ_i for values of $\epsilon \ll 1$ as

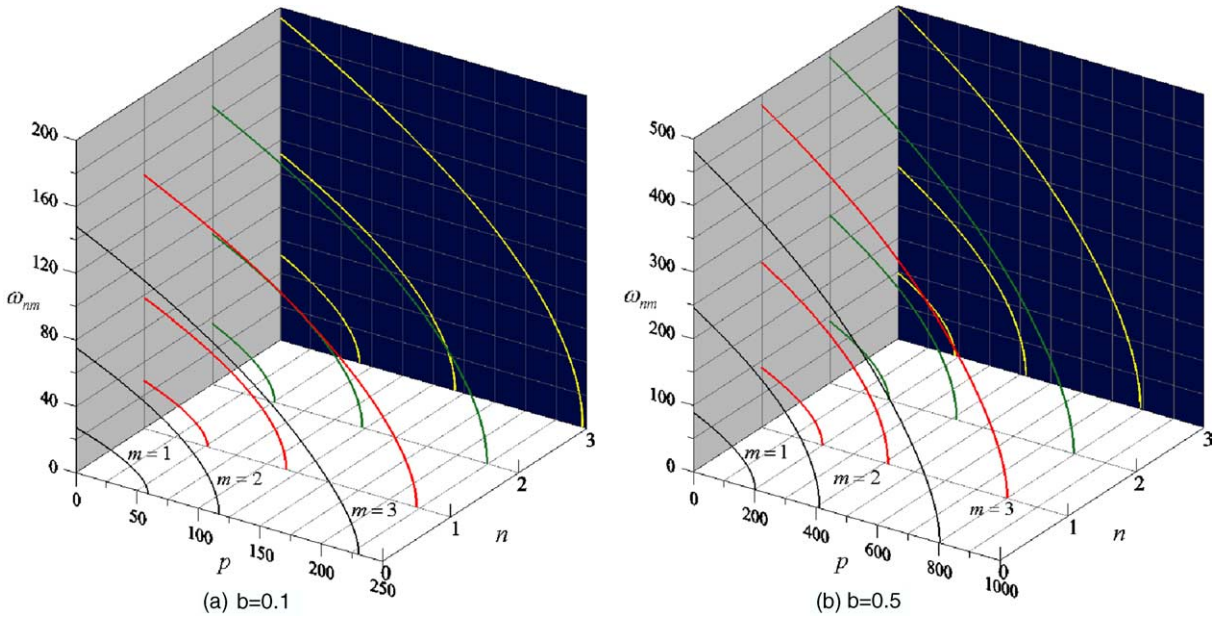

Fig. 9. Variation of the first few natural frequencies ω_{nm} with the thermal load p when $\tau = 0.5$.

Table 4
Values of the first few critical buckling loads p^*_{nm} of two annular plates for the case $\tau = 0.5$

n	$b = 0.1$			$b = 0.5$		
	p^*_{n1}	p^*_{n2}	p^*_{n3}	p^*_{n1}	p^*_{n2}	p^*_{n3}
0	58.804	116.780	230.678	201.584	412.002	803.846
1	51.777	116.018	222.450	198.941	412.643	801.554
2	50.995	122.496	224.259	192.801	414.779	796.536
3	64.772	142.742	246.875	187.156	418.973	792.588

$$\xi_i = \sqrt{\omega_{nm}}\sqrt{\pm\frac{1}{2}\epsilon + \sqrt{\left(\frac{1}{2}\epsilon\right)^2 + 1}} \approx \sqrt{\omega_{nm}}\left(1 \pm \frac{1}{4}\epsilon\right). \tag{50}$$

Subsequently, the term $\tilde{\nabla}^4\phi_{nm}/(\omega^2_{nm}\phi_{nm}) = \mathrm{O}(1)$ while the term $p\tilde{\nabla}^2\phi_{nm}/(\omega^2_{nm}\phi_{nm}) = \mathrm{O}(\epsilon)$.

Therefore, for values of $p \ll \omega_{nm}$, we propose to use the method of strained parameters (Nayfeh, 1981) to obtain approximate closed-form solutions to the nondimensional eigenvalue problem. To this end, we assume the mode shapes and natural frequencies of the plate to be equal to those of an unheated plate with small perturbations added to them. That is, we let

$$\phi^*_{nm}(r) = \phi_{nm[0]}(r) + \epsilon\phi_{nm[1]}(r) + \cdots, \tag{51}$$

$$\omega^*_{nm} = \omega_{nm[0]} + \epsilon\omega_{nm[1]} + \cdots, \tag{52}$$

where the "asterisk" indicates approximate solutions of the nondimensional mode shapes and natural frequencies.

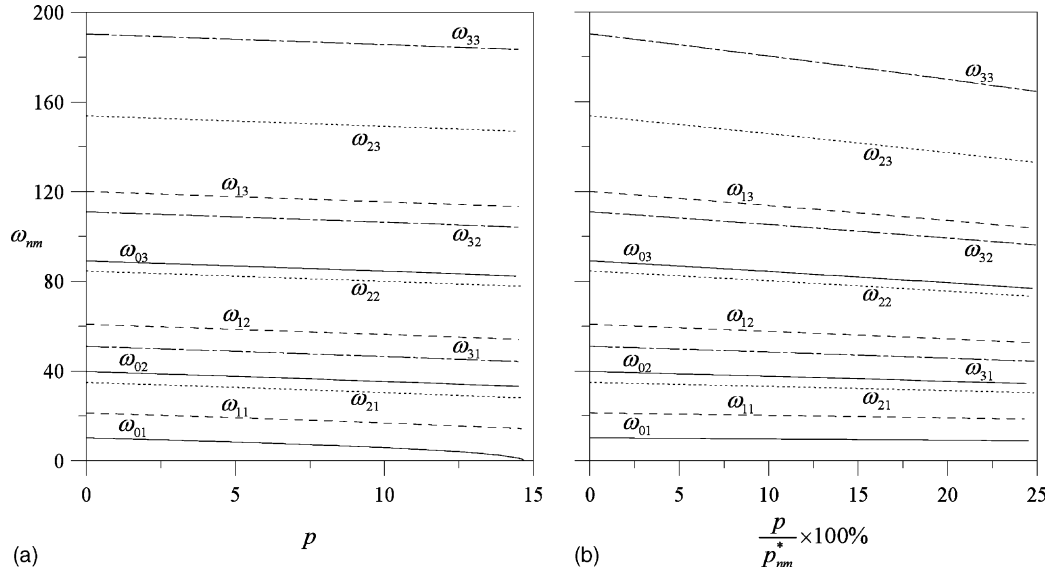

Fig. 10. Variation of the first few natural frequencies for a circular plate ($b = 0$) with the thermal load p for up to (a) the lowest buckling load $p^*_{01} = 14.682$ and (b) 25% of the corresponding buckling load p^*_{nm}.

8.1. Case of $b = 0$: a circular plate

We set $p = \epsilon\omega_{nm}$ and substitute Eqs. (51) and (52) into Eq. (39), the boundary conditions at $r = 1$ in Eq. (37), and the constraint $\phi(r) < \infty$ at $r = 0$. Then, after separating the terms of equal powers of ϵ, we obtain the following hierarchy of boundary-value problems:

$$\tilde{\nabla}^4\phi_{[0]} - \omega^2_{[0]}\phi_{[0]} = 0, \tag{53}$$

$$\tilde{\nabla}^4\phi_{[1]} - \omega^2_{[0]}\phi_{[1]} = 2\omega_{[0]}\omega_{[1]}\phi_{[0]} - \omega_{[0]}\tilde{\nabla}^2\phi_{[0]}, \tag{54}$$

where the subscript nm has been temporarily dropped for convenience. The corresponding boundary conditions are $\phi_{[k]} < \infty$ at $r = 0$ and

$$\phi_{[k]} = 0 \quad \text{and} \quad \frac{\mathrm{d}\phi_{[k]}}{\mathrm{d}r} = 0 \quad \text{at } r = 1 \tag{55}$$

for $k = 0, 1$.

The solution of the first-order problem, corresponding to the unheated plate, can be expressed as

$$\phi_{[0]}(r) = D_1 J_n\left(\sqrt{\omega_{[0]}}r\right) + D_2 Y_n\left(\sqrt{\omega_{[0]}}r\right) + D_3 I_n\left(\sqrt{\omega_{[0]}}r\right) + D_4 K_n\left(\sqrt{\omega_{[0]}}r\right), \tag{56}$$

where $D_2 = D_4 = 0$ to satisfy the constraint at $r = 0$. The coefficients D_1 and D_3 and the natural frequencies of the unheated circular plate $\omega_{[0]}$ are determined from

$$\begin{bmatrix} J_n\left(\sqrt{\omega_{[0]}}\right) & I_n\left(\sqrt{\omega_{[0]}}\right) \\ \sqrt{\omega_{[0]}}J'_n\left(\sqrt{\omega_{[0]}}\right) & \sqrt{\omega_{[0]}}I'_n\left(\sqrt{\omega_{[0]}}\right) \end{bmatrix} \begin{Bmatrix} D_1 \\ D_3 \end{Bmatrix} = \begin{Bmatrix} 0 \\ 0 \end{Bmatrix} \tag{57}$$

and the normalization constraint $\int_0^1 r\phi^2_{[0]}\,\mathrm{d}r = 1$. In Eq. (57), the "$'$" denotes the derivative with respect to the argument $\sqrt{\omega_{[0]}}r$.

Next, we substitute the results for $\phi_{[0]}(r)$ and $\omega_{[0]}$ into Eq. (54). Since the resulting homogeneous problem in Eq. (54) is the same as Eq. (53), we find that nontrivial solutions of the nonhomogeneous problem in

Eq. (54) exist only if a solvability condition is satisfied (Nayfeh, 1981). Towards this end, we multiply Eq. (54) by the $r\eta(r)$, where $\eta(r)$ is the solution of the adjoint problem, integrate by parts until all of the derivatives are transferred from $\phi_{[1]}$ to η, apply the boundary conditions on $\phi_{[1]}$, find that $\eta = \phi_{[0]}$ and, consequently, arrive at the solvability condition

$$\omega_{[1]} = \frac{1}{2}\int_0^1 r\phi_{[0]}\tilde{\nabla}^2\phi_{[0]}\,\mathrm{d}r. \tag{58}$$

Therefore, it follows from Eqs. (52) and (58) that, to first-order, the natural frequencies of the heated circular plate for $p \ll \omega_{nm}$ are approximately given by

$$\omega^*_{nm} \approx \omega_{nm[0]} + \frac{p}{2\omega_{nm[0]}}\int_0^1 r\phi_{nm[0]}\tilde{\nabla}^2\phi_{nm[0]}\,\mathrm{d}r, \tag{59}$$

where ϵ is replaced with $\dfrac{p}{\omega_{nm[0]}}$.

In Fig. 11, we present the percent errors

$$\mathrm{Err}_{nm} = \left|\frac{\omega_{nm} - \omega^*_{nm}}{\omega_{nm}}\right| \times 100\% \tag{60}$$

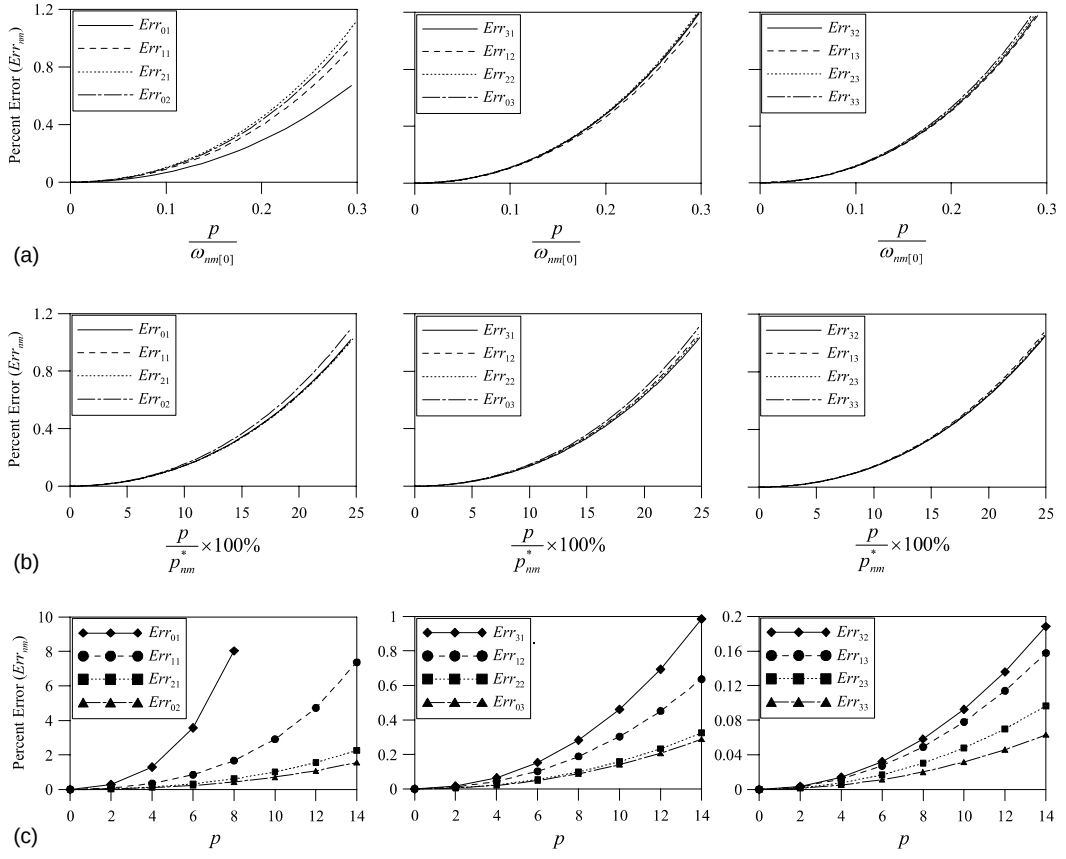

Fig. 11. Variation of the percent errors, Err_{nm}, of the approximate natural frequencies for a circular plate (i.e., $b = 0$) with (a) the small parameter $\epsilon \equiv \frac{p}{\omega_{nm[0]}}$, (b) $p \leqslant 25\%$ of p^*_{nm}, and (c) p up to the lowest buckling load $p^*_{01} = 14.682$.

resulting from using Eq. (59) to estimate the natural frequencies, relative to those obtained numerically, as the thermal load p is varied. In part (a), we present the percent errors in terms of the parameter $\epsilon \equiv \frac{p}{\omega_{nm[0]}}$. Although the solution in Eq. (59) was obtained for $\epsilon \ll 1$, we find very good agreement of up to $\mathrm{Err}_{nm} \leqslant 1.2\%$ for values of $\epsilon \leqslant 0.3$. In part (b), we present the percent errors in terms of the thermal load ratio $\frac{p}{p^*_{nm}}$. Again, there is very good agreement of up to $\mathrm{Err}_{nm} \leqslant 1.2\%$ for values of $p \leqslant 25\%$ of p^*_{nm}. In part (c), we present the percent errors in terms of $p \leqslant p^*_{01}$ (the lowest buckling load) and conclude that the accuracy of the approximation increases for increasing natural frequencies $\omega_{nm[0]}$ of the unheated plate.

8.2. Case of $b \neq 0$: an annular plate

Although for the general problem, where τ may be different from unity, closed-form solutions are not yet available, one may surmise from the previous numerical results that a similar argument for ordering the different terms in Eq. (36) could be made. This is because the solutions of the general problem can be expressed in terms of the Bessel functions in Eq. (40) as

$$\phi_{nm}(r) = \sum_{l=1}^{\infty}[A_{1l}J_l(\xi_1 r) + A_{2l}Y_l(\xi_1 r) + A_{3l}I_l(\xi_2 r) + A_{4l}K_l(\xi_2 r)],$$

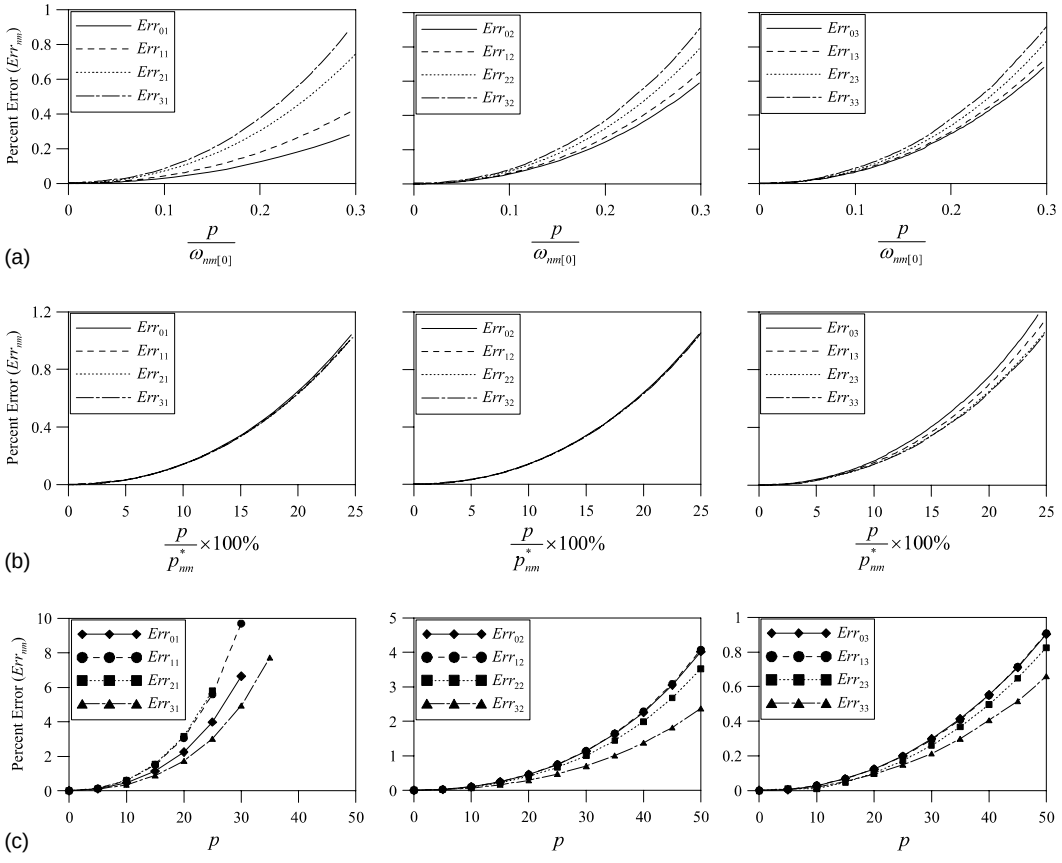

Fig. 12. Variation of the percent errors, Err_{nm}, of the approximate natural frequencies, for an annular plate having $b = 0.1$ and $\tau = 0.5$, with (a) the small parameter $\epsilon \equiv \frac{p}{\omega_{nm[0]}}$, (b) $p \leqslant 25\%$ of p^*_{nm}, and (c) p up to the lowest buckling load $p^*_{21} = 50.995$.

where the ξ_i are given by Eq. (50). Therefore, substituting the expansions in Eqs. (51) and (52) into Eq. (36), setting $\epsilon \equiv \frac{p}{\omega_{nm}}$, and separating terms of equal powers of ϵ, we obtain Eq. (53) and

$$\tilde{\nabla}^4\phi_{[1]} - \omega_{[0]}^2\phi_{[1]} = 2\omega_{[0]}\omega_{[1]}\phi_{[0]} - \omega_{[0]}\left\{\frac{1}{r}\frac{\mathrm{d}}{\mathrm{d}r}\left[L_1(r)\frac{\mathrm{d}\phi_{[0]}}{\mathrm{d}r}\right] - \frac{n^2}{r^2}L_2(r)\phi_{[0]}\right\}. \tag{61}$$

The solution of the first-order problem is given by Eq. (56) where the coefficients $D_1 - D_4$ and natural frequencies $\omega_{[0]}$ of the unheated annular plate are determined from

$$\begin{bmatrix} J_n\left(\sqrt{\omega_{[0]}}b\right) & Y_n\left(\sqrt{\omega_{[0]}}b\right) & I_n\left(\sqrt{\omega_{[0]}}b\right) & K_n\left(\sqrt{\omega_{[0]}}b\right) \\ \sqrt{\omega_{[0]}}J_n'\left(\sqrt{\omega_{[0]}}b\right) & \sqrt{\omega_{[0]}}Y_n'\left(\sqrt{\omega_{[0]}}b\right) & \sqrt{\omega_{[0]}}I_n'\left(\sqrt{\omega_{[0]}}b\right) & \sqrt{\omega_{[0]}}K_n'\left(\sqrt{\omega_{[0]}}b\right) \\ J_n\left(\sqrt{\omega_{[0]}}\right) & Y_n\left(\sqrt{\omega_{[0]}}\right) & I_n\left(\sqrt{\omega_{[0]}}\right) & K_n\left(\sqrt{\omega_{[0]}}\right) \\ \sqrt{\omega_{[0]}}J_n'\left(\sqrt{\omega_{[0]}}\right) & \sqrt{\omega_{[0]}}Y_n'\left(\sqrt{\omega_{[0]}}\right) & \sqrt{\omega_{[0]}}I_n'\left(\sqrt{\omega_{[0]}}\right) & \sqrt{\omega_{[0]}}K_n'\left(\sqrt{\omega_{[0]}}\right) \end{bmatrix} \begin{Bmatrix} D_1 \\ D_2 \\ D_3 \\ D_4 \end{Bmatrix} = \begin{Bmatrix} 0 \\ 0 \\ 0 \\ 0 \end{Bmatrix} \tag{62}$$

and the normalization constraint $\int_b^1 r\phi_{[0]}^2\,\mathrm{d}r = 1$. Then, substituting the results for $\phi_{[0]}(r)$ and $\omega_{[0]}$ into Eq. (61), solving for the adjoint $\eta(r) = \phi_{[0]}(r)$, and determining the solvability condition, we find that, to first-order, the natural frequencies of the heated annular plate for $p \ll \omega_{nm}$ are approximately given by

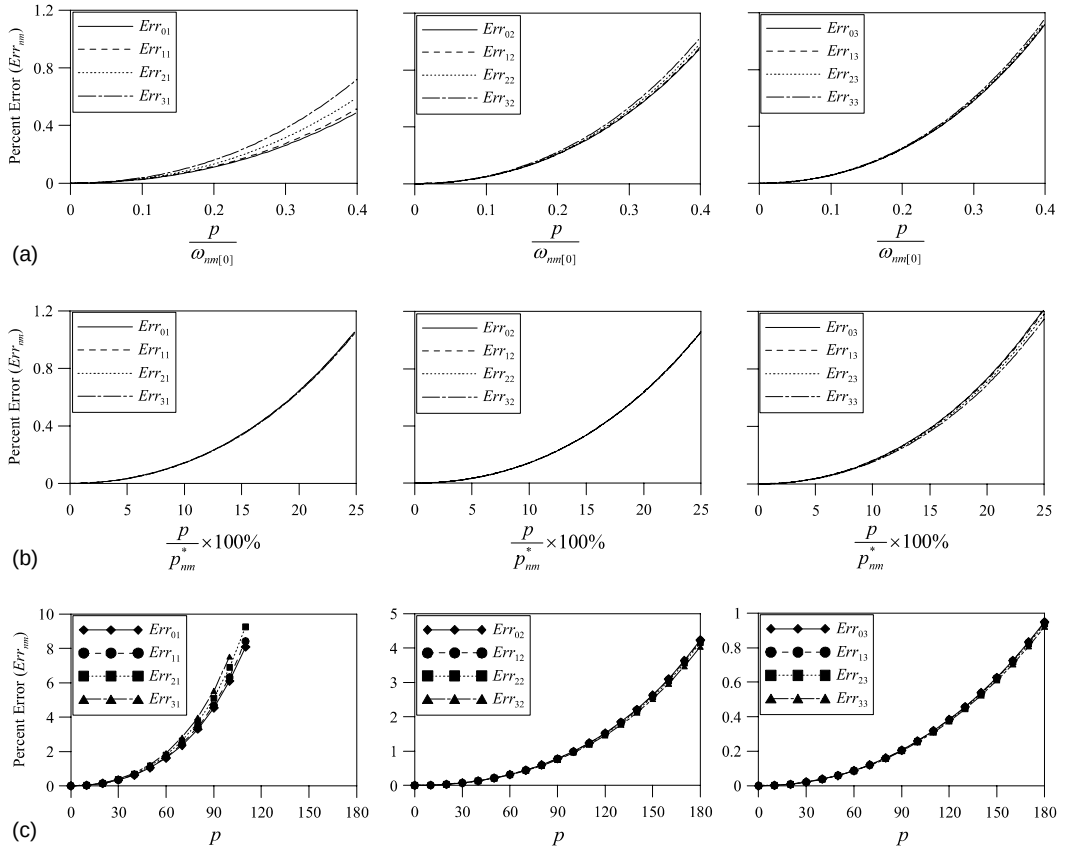

Fig. 13. Variation of the percent errors, Err_{nm}, of the approximate natural frequencies, for an annular plate having $b = 0.5$ and $\tau = 0.5$, with (a) the small parameter $\epsilon \equiv \frac{p}{\omega_{nm[0]}}$, (b) $p \leqslant 25\%$ of p^*_{nm}, and (c) p up to the lowest buckling load $p^*_{31} = 187.156$.

$$\omega^*_{nm} \approx \omega_{nm[0]} + \frac{p}{2\omega_{nm[0]}} \int_b^1 r\phi_{nm[0]} \left\{ \frac{1}{r} \frac{\mathrm{d}}{\mathrm{d}r} \left[L_1(r) \frac{\mathrm{d}\phi_{nm[0]}}{\mathrm{d}r} \right] - \frac{n^2}{r^2} L_2(r) \phi_{nm[0]} \right\} \mathrm{d}r. \tag{63}$$

In Figs. 12 and 13, we present the percent errors Err_{nm} resulting when using Eq. (63) to estimate the natural frequencies, relative to those obtained numerically, for annular plates with $b = 0.1$ and 0.5,

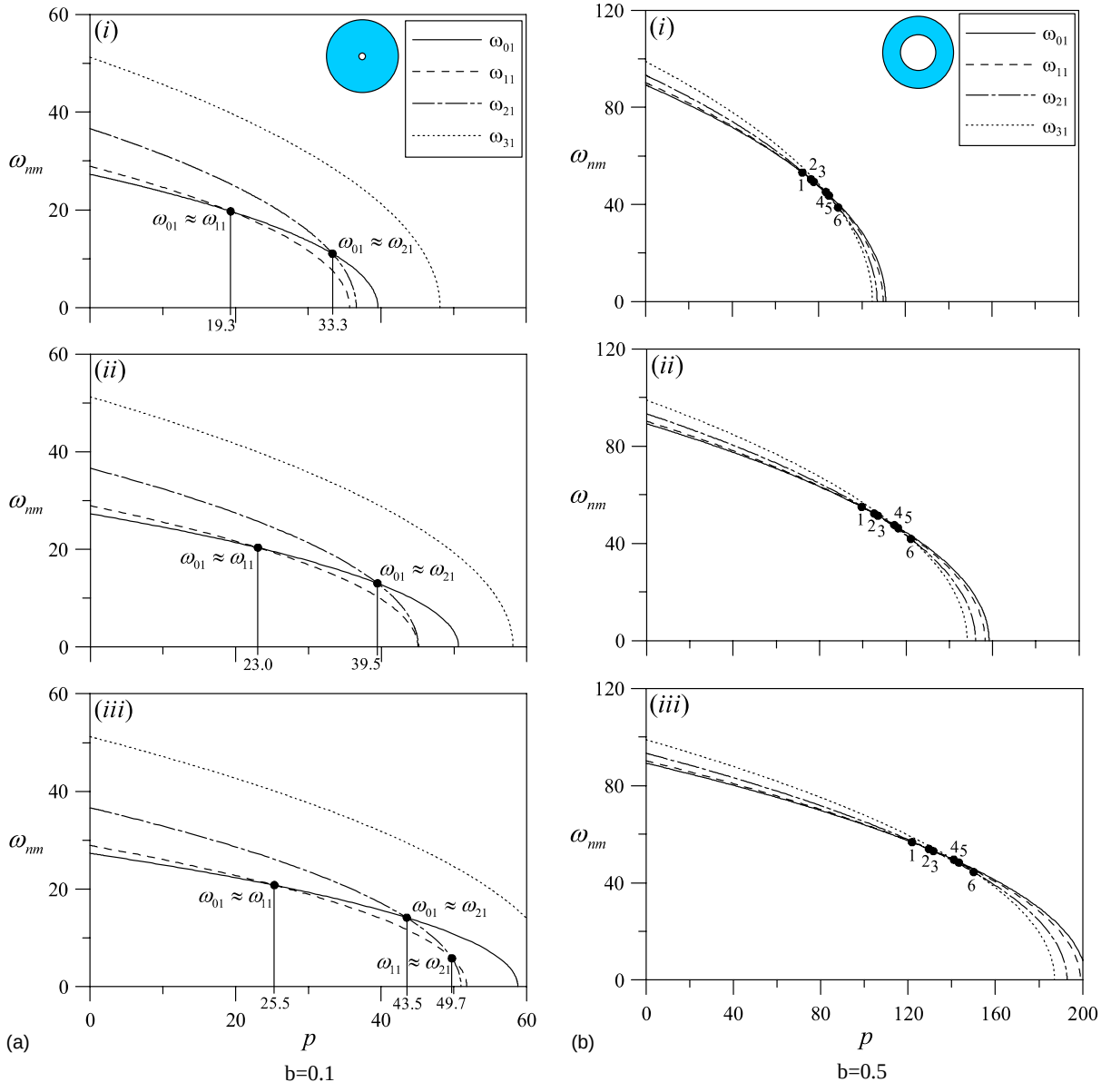

Fig. 14. Variation of the lowest four natural frequencies (ω_{01}, ω_{11}, ω_{21}, ω_{31}) for two annular plates with the thermal load p for the three cases: (i) $\tau = 2$, (ii) $\tau = 1$, and (iii) $\tau = 0.5$. The numbers 1–6 in part (b) denote the resonances $\omega_{01} \approx \omega_{11}$, $\omega_{01} \approx \omega_{21}$, $\omega_{11} \approx \omega_{21}$, $\omega_{01} \approx \omega_{31}$, $\omega_{11} \approx \omega_{31}$, and $\omega_{21} \approx \omega_{31}$, respectively.

respectively. In both cases, the value of $\tau = 0.5$. Again, we note that the approximate solution of Eq. (63) exhibits similar trends to those discussed for the circular plate in the previous section.

9. Modal interactions

We mentioned earlier that, as p varies, internal resonances involving different modes may be activated. This, in turn, could lead to complex and sometimes undesirable vibrations if the plate is under an external excitation, as it may be the case in many applications having such a component. If follows from Figs. 5 and 7 that three-to-one and combination internal resonances may be activated among modes having the same number n of nodal diameters. Moreover, the results in Fig. 5 are qualitatively true for values of $\tau \neq 1$.

In addition, one-to-one internal resonances between modes having the same number m of nodal circles may be activated in annular plates. For example, in Fig. 14a, we present the variation of the natural frequencies ω_{01}, ω_{11}, ω_{21}, and ω_{31} with p when $b = 0.1$ for (i) $\tau = 2$, (ii) $\tau = 1$, and (iii) $\tau = 0.5$. As p is increased, we find that the one-to-one internal resonances $\omega_{01} \approx \omega_{11}$ and $\omega_{01} \approx \omega_{21}$ may be activated, as shown for $\tau = 2$. Setting $\tau = 1$, we obtain a similar behavior, but with the two internal resonances shifted to the right in p. In such cases, vibrations of the plate could consist of both standing and traveling waves. Reducing τ to 0.5, we find that a third one-to-one internal resonance $\omega_{11} \approx \omega_{21}$ may also be activated.

We increase the ratio of the inner radius to the outer radius to $b = 0.5$ and present once more in Fig. 14b the variation of ω_{01}, ω_{11}, ω_{21}, and ω_{31} with p for (i) $\tau = 2$, (ii) $\tau = 1$, and (iii) $\tau = 0.5$. In this case, the natural frequencies are closer to each other, resulting in six different combinations of one-to-one internal resonances: $\omega_{01} \approx \omega_{11}$, $\omega_{01} \approx \omega_{21}$, $\omega_{11} \approx \omega_{21}$, $\omega_{01} \approx \omega_{31}$, $\omega_{11} \approx \omega_{31}$, and $\omega_{21} \approx \omega_{31}$. They are numbered 1–6, respectively, in Fig. 14b and the corresponding values of p are presented in Table 5. We find that the resonances are clustered relatively close to each other, such that two or more of them may be activated simultaneously, possibly resulting in three- or four-mode interactions.

10. Summary

We investigated the mode shapes and natural frequencies of circular and annular plates under axisymmetric steady-state thermal loads. We formulated the problem by using a linearized version of the von Kármán plate theory and the heat conduction equation. We neglected the influence of the thermoelastic coupling term and solved the heat conduction equation for the steady-state temperature distribution. Then, we solved the compatibility equation for the stress function and substituted the result into the equation of motion to obtain the eigenvalue problem.

Table 5
Values of p for which the one-to-one internal resonances 1–6 in Fig. 14b may occur

#	Resonance	p		
		$\tau = 2$	$\tau = 1$	$\tau = 0.5$
1	$\omega_{01} \approx \omega_{11}$	72.3	99.0	122.4
2	$\omega_{01} \approx \omega_{21}$	76.4	105.1	129.3
3	$\omega_{11} \approx \omega_{21}$	77.8	107.0	131.7
4	$\omega_{01} \approx \omega_{31}$	83.4	114.6	140.9
5	$\omega_{11} \approx \omega_{31}$	84.8	116.5	143.3
6	$\omega_{21} \approx \omega_{31}$	88.9	122.1	150.2

We presented and analyzed two cases where closed-form solutions exist: an annular plate under a zero temperature gradient and a circular plate. Furthermore, we used a shooting method to numerically solve and analyze cases of nonzero temperature gradients. We studied the influence of the thermal load p, the ratio τ of the absolute temperatures at the boundaries, and the ratio b of the inner radius to the outer radius on the natural frequencies of the system. We found that, as the thermal load is increased, the natural frequencies monotonously decrease to zero, causing the plate to buckle. When the temperature at the inner boundary is greater than that at the outer boundary (i.e., $\tau > 1$), a lower thermal load will cause buckling, and vice versa. Furthermore, with an increase in the ratio b, the natural frequencies increase and larger thermal loads are needed to cause buckling.

For values of $p \ll \omega_{nm}$, we used the method of strained parameters to obtain approximate closed-form expressions for the natural frequencies. We showed, by examples for both circular and annular plates, that these approximations can yield very accurate results, especially for the higher natural frequencies for values of p up to the lowest buckling level.

Varying the thermal load, we found that several types of internal resonances may be activated. For example, in annular and circular plates, we found that three-to-one and combination internal resonances may occur among modes having the same number n of nodal diameters. Arafat and Nayfeh (2003) investigated the nonlinear responses of clamped–clamped thermally loaded annular plates in the presence of a three-to-one internal resonance between the second and first axisymmetric modes (i.e., $\omega_{02} \approx 3\omega_{01}$) when the second mode is excited near primary resonance (i.e., $\Omega \approx \omega_{02}$). They used a combination of a numerical shooting technique and the method of multiple scales to obtain approximate solutions and found that two-mode periodic vibrations of the plate with a large component from the first mode occur, appearing as isolated solutions "islands" in the force- and frequency-response curves. Moreover, two-mode quasiperiodic vibrations of the plate can develop through Hopf bifurcations.

Furthermore, in annular plates, modes with the same number m of nodal circles exhibit frequency crossovers, and hence one-to-one internal resonances. For larger values of b, these crossovers occur closer to each other, and hence simultaneous one-to-one internal resonances might be activated. An interesting consequence of the frequency crossovers is that the first buckling shape of an annular plate may not be in the form of the mode shape of the lowest natural frequency in the absence of heat. For example, if ω_{01} is the lowest natural frequency when $p = 0$, the plate may first buckle at $p = p_{11}^*$ (and not p_{01}^*) in the shape of the asymmetric mode $\phi_{11}(r)e^{i\theta}$ due to the frequency crossing between ω_{01} and ω_{11}, as evident from Fig. 14a for the case of $\tau = 2$. In other cases, the first buckling shape may be in the form of the mode $\phi_{21}e^{2i\theta}$, as demonstrated by Fig. 14a for the cases of $\tau = 1$ and 0.5, and the mode $\phi_{31}e^{3i\theta}$, as demonstrated by Fig. 14b for all three cases.

References

Arafat, H.N., Nayfeh, A.H., 2003. Modal interactions in a thermally loaded annular plate. In: Proceedings of the 2003 ASME Design Engineering Technical Conferences, September 2–6, DETC03/VIB-48603. Chicago, IL, pp. 1–10.

Boley, B.A., Weiner, J.H., 1960. Theory of Thermal Stresses. Wiley, New York.

Fedorov, V.A., 1976. Thermostability of elastically clamped variable-stiffness annular plates. Soviet Aeronautics 19, 105–109.

Hetnarski, R.B., 1987. Thermal Stresses II. North-Holland, Amsterdam.

Irie, T., Yamada, G., 1978. Thermally induced vibration of circular plate. Bulletin of the JSME 21, 1703–1709.

Li, S.-R., Zhou, Y.-H., Song, X., 2002. Non-linear vibration and thermal buckling of an orthotropic annular plate with a centric rigid mass. Journal of Sound and Vibration 251, 141–152.

Mote, C.D., 1965. Free vibration of initially stressed circular disks. Journal of Engineering for Industry 87, 258–264.

Mote, C.D., 1966. Theory of thermal natural frequency variations in disks. International Journal of Mechanical Sciences 8, 547–557.

Mote, C.D., 1967. Natural frequencies in annuli with induced thermal membrane stresses. Journal of Engineering for Industry 89, 611–618.

Nayfeh, A.H., 1981. Introduction to Perturbation Techniques. Wiley, New York.

Newman, M., Forray, M., 1962. Axisymmetric large deflections of circular plates subjected to thermal and mechanical loads. Journal of the Aerospace Sciences 29, 1060–1066.

Stodola, A., 1924. Dampf- und Gas-Turbinen, sixth ed. Springer, Berlin (Translated from German by Loewenstein, L.C., 1927. Steam and Gas Turbines. McGraw-Hill, New York).

Thornton, E.A., 1993. Thermal buckling of plates and shells. Applied Mechanics Reviews 46, 485–506.

von Freudenreich, J., 1925. Vibration of steam turbine discs. Engineering 119, 2–4, 31–34.